
Volume 166, issues 17–18, 18 September 2011 ISSN: 0377-0257
ELSEVIER
Journal of Non~Newtonian Fluid Mechanics
On-line Access via:
www.elsevier.com/locate/jnnfm

Journal of Non-Newtonian Fluid Mechanics 166 (2011) 1049–1063

Contents lists available at ScienceDirect

Journal of Non-Newtonian Fluid Mechanics

journal homepage: http://www.elsevier.com/locate/jnnfm

Laminar natural convection of power-law fluids in a square enclosure with differentially heated side walls subjected to constant temperatures

Osman Turan [a,b], Anuj Sachdeva [a], Nilanjan Chakraborty [a], Robert J. Poole [a,*]

[a] School of Engineering, University of Liverpool, Brownlow Hill, Liverpool L69 3GH, UK
[b] Department of Mechanical Engineering, Karadeniz Technical University, Trabzon 61080, Turkey

ARTICLE INFO

Article history:
Received 1 March 2011
Received in revised form 6 April 2011
Accepted 5 June 2011
Available online 12 June 2011

Keywords:
Power-law model
Natural convection
Heat transfer
Finite-volume

ABSTRACT

Two-dimensional steady-state simulations of laminar natural convection in square enclosures with differentially heated sidewalls subjected to constant wall temperatures have been carried out where the enclosures are considered to be completely filled with non-Newtonian fluids obeying the power-law model. The effects of power-law index n in the range $0.6 \leqslant n \leqslant 1.8$ on heat and momentum transport are investigated for nominal values of Rayleigh number (Ra) in the range 10^3–10^6 and a Prandtl number (Pr) range of 10–10^5. It is found that the mean Nusselt number $\overline{Nu}$ increases with increasing values of Rayleigh number for both Newtonian and power-law fluids. However, $\overline{Nu}$ values obtained for power-law fluids with $n < 1$ ($n > 1$) are greater (smaller) than that obtained in the case of Newtonian fluids with the same nominal value of Rayleigh number Ra due to strengthening (weakening) of convective transport. With increasing shear-thickening (i.e. $n > 1$) the mean Nusselt number $\overline{Nu}$ settles to unity ($\overline{Nu} = 1.0$) as heat transfer takes place principally due to thermal conduction. The effects of Prandtl number have also been investigated in detail and physical explanations are provided for the observed behaviour. New correlations are proposed for the mean Nusselt number $\overline{Nu}$ for both Newtonian and power-law fluids which are shown to satisfactorily capture the correct qualitative and quantitative behaviour of $\overline{Nu}$ in response to changes in Ra, Pr and n.

1. Introduction

Natural convection in rectangular enclosures with differentially heated vertical sidewalls and adiabatic horizontal walls is one of the most extensively studied configurations for Newtonian flows [1–3]. The extensive review of Ostrach [4] neatly captures the available data up to that date. In addition to the obvious fundamental interest, this configuration has engineering relevance in solar collectors, food preservation, compact heat exchangers and electronic cooling systems. In comparison to the vast body of literature regarding the natural convection of Newtonian fluids, a comparatively limited effort has been directed towards understanding of natural convection of non-Newtonian fluids in rectangular enclosures. The Rayleigh–Bénard configuration [5], which classically involves a rectangular enclosure with adiabatic vertical walls and differentially heated horizontal walls with the bottom wall at higher temperature, has been investigated for a range of different non-Newtonian models including inelastic Generalised Newtonian Fluids (GNF) [6–9], fluids with a yield stress [10–12] and viscoelastic fluids [13].

Kim et al. [14] studied transient natural convection of non-Newtonian power-law fluids (power-law index $n \leqslant 1$) in a square enclosure with differentially heated vertical side walls subjected to constant wall temperatures. They studied a range of nominal Rayleigh numbers from $Ra_K = 10^5$–10^7 and Prandtl numbers from $Pr_K = 10^2$–10^4 and demonstrated that the mean Nusselt number $\overline{Nu}$ increases with decreasing power-law index n for a given set of values of Ra_K and Pr_K.[1] This result is consistent with the numerical findings of Ohta et al. [8] where the Sutterby model was used for analysing transient natural convection of shear-thinning fluids in the Rayleigh–Bénard configuration. The augmentation of the strength of natural convection in rectangular enclosures for shear-thinning fluids was also confirmed by both experimental and numerical studies on micro-emulsion slurries by Inaba et al. [9] in the Rayleigh–Bénard configuration. Lamsaadi et al. [15,16] have studied the effects of the powerlaw index on natural convection in the high Prandtl number limit for both tall [15] and shallow enclosures [16] where the sidewall boundary conditions are subjected to constant heat fluxes (rather than isothermal as in the cases discussed above). Lamsaadi

* Corresponding author. Tel.: +44 1517944806; fax: +44 1517944848.
E-mail addresses: osmanturan@ktu.edu.tr (O. Turan), a.sachdeva@liv.ac.uk (A. Sachdeva), n.chakraborty@liv.ac.uk (N. Chakraborty), robpoole@liv.ac.uk (R.J. Poole).

[1] The definitions of Ra_k and Pr_k are provided later in Section 2.

0377-0257/$ - see front matter © 2011 Elsevier B.V. All rights reserved.
doi:10.1016/j.jnnfm.2011.06.003

Nomenclature

c_p	specific heat at constant pressure (J/kg K)
e	relative error (–)
e_{ij}	rate of strain tensor (s^{-1})
F_s	factor of safety (–)
g	gravitational acceleration (m/s^2)
Gr	Grashof number (–)
h	heat transfer coefficient (W/m^2 K)
K	consistency ($N\ s^n/m^2$)
k	thermal conductivity (W/m K)
L	length and height of the enclosure (m)
n	power-law index (–)
Pr	Prandtl number
q	heat flux (W/m^2)
r	ratio between the coarse to fine grid spacings (–)
r_e	grid expansion ratio (–)
Ra	Rayleigh number (–)
T	temperature (K)
t	time (s)
u_i	ith velocity component (m/s)
U,V	dimensionless horizontal ($U = u_1L/\alpha$) and vertical velocity ($V = u_2L/\alpha$) (–)
ϑ	characteristic velocity (m/s)
x_i	coordinate in ith direction (m)
α	thermal diffusivity (m^2/s)
β	coefficient of thermal expansion (1/K)
δ,δ_{th}	velocity and thermal boundary-layer thickness (m)
θ	dimensionless temperature ($\theta = (T - T_C)/(T_H - T_C)$) (–)
μ	dynamic viscosity (N s/m^2)
ν	kinematic viscosity (m^2/s)
ρ	density (kg/m^3)
τ_{ij} (τ)	stress tensor (stress) (Pa)
ϕ	general primitive variable (–)
ψ	dimensionless stream function (–)
Subscripts	
a	apparent
C	cold wall
$char$	characteristic value
eff	effective value
ext	extrapolated value
H	hot wall
K	based on definitions given in [14]
max	maximum value
nom	nominal value
ref	reference value
$wall$	wall value
Special characters	
ΔT	difference between hot and cold wall temperature (= (T_H-T_C)) (K)
$\Delta_{\min,cell}$	minimum cell distance (m)

et al. [15,16] show that the convective heat transfer rate becomes dependent only on nominal Rayleigh number Ra and the power-law index n for large values of aspect ratio and the nominal Prandtl number Pr.[1] Barth and Carey [17] utilised GNF models which incorporate limiting viscosities at low and high shear rates to study a three-dimensional version of the problem (the adiabatic boundary conditions are replaced by a linear variation in temperature to match the experimental conditions of [18]). Recently Vola et al. [19] and the present authors [20,21] numerically studied steady two-dimensional natural convection of yield stress fluids obeying the Bingham model in rectangular enclosures with differentially heated vertical side walls and proposed correlations for the mean Nusselt number $\overline{Nu}$.

In the present study steady natural convection of Ostwald–De Waele (i.e. power-law) fluids in a square enclosure with differentially heated side walls subjected to constant wall temperatures has been studied numerically. A parametric study has been conducted with the power-law index n ranging from 0.6 to 1.8 for a range of nominal values of Rayleigh and Prandtl numbers (definitions are provided in Section 2) given by $Ra = 10^3{-}10^6$ and $Pr = 10{-}10^5$. The simulation data in turn has been used to develop a correlation for the mean Nusselt number $\overline{Nu}$ based on a detailed scaling analysis for the broad range of n, Ra and Pr considered in this study. In this respect the main objectives of the present paper are as follows:

(1) To demonstrate the effects of n, Ra and Pr on the mean Nusselt number $\overline{Nu}$ in the case of natural convection of power-law fluids in a square enclosure with differentially heated vertical side walls subjected to constant wall temperatures.
(2) To elucidate the above effects with the aid of a detailed scaling analysis.
(3) To develop a correlation for the mean Nusselt number for natural convection of power-law fluids in a square differentially heated vertical side walls subjected to constant wall temperatures.

The rest of the paper will be organised as follows. The necessary mathematical background and numerical details will be presented in the next section, which will be followed by the scaling analysis. Following this analysis, the results will be presented and subsequently discussed. The main findings will be summarised and conclusions will be drawn in the final section of this paper.

2. Mathematical background and numerical implementation

2.1. Non-dimensional numbers

For the Ostwald–De Waele (i.e. power law) model the viscous stress tensor τ_{ij} is given by:

$$\tau_{ij} = \mu_a e_{ij} = K(e_{kl}e_{kl}/2)^{(n-1)/2} e_{ij}, \tag{1}$$

where $e_{ij} = (\partial u_i/\partial x_j + \partial u_j/\partial x_i)$ is the rate of strain tensor, K is the consistency, n is the power-law index and μ_a is the apparent viscosity which is given by:

$$\mu_a = K(e_{kl}e_{kl}/2)^{(n-1)/2}. \tag{2}$$

For $n < 1$ ($n > 1$) the apparent viscosity decreases (increases) with increasing shear rate and thus the fluids with $n < 1$ ($n > 1$) are referred to as shear-thinning (shear-thickening) fluids. In the present study, natural convection of power-law fluids in a square enclosure (of dimension L) with differentially heated constant temperature side walls filled with power-law fluids is compared with the heat transfer rate obtained for different values of n with the same nominal values of Rayleigh number and Prandtl number. The nominal Rayleigh number Ra_{nom} represents the ratio of the strengths of thermal transport due to the buoyancy force to that due to thermal diffusion, which is defined here as:

$$Ra_{nom} = \frac{\rho^2 c_p g\beta\Delta T L^3}{\mu_{nom} k} = Gr_{nom}Pr_{nom}, \tag{3}$$

where Gr_{nom} is the nominal Grashof number and Pr_{nom} is the nominal Prandtl number, which are defined as:

$$Gr_{nom} = \frac{\rho^2 g\beta\Delta T L^3}{\mu_{nom}^2} \quad \text{and} \quad Pr_{nom} = \frac{\mu_{nom} c_p}{k}. \tag{4}$$

The Grashof number represents the ratio of the strengths of the buoyancy and viscous forces while the Prandtl number depicts the ratio of the strengths of momentum diffusion to thermal diffusion. Alternatively, the Prandtl number can be taken to represent the ratio of the viscous boundary-layer to thermal boundary-layer thicknesses.

For power-law fluids – because the viscosity varies with the flow – in Eqs. (3) and (4) μ_{nom} represents the value of "nominal" viscosity. An important consideration in heat and fluid flow problems for power-law fluids lies in the most appropriate choice of this nominal viscosity. The nominal viscosity μ_{nom} can be defined based on a characteristic shear rate $\dot{\gamma}$ which can itself be scaled as: $\dot{\gamma} \sim u_{char}/L$ where u_{char} is a characteristic velocity scale. Using a characteristic velocity scale given by $u_{char} \sim \alpha/L$ as in Refs. [15,16,22], one can obtain the following expression for μ_{nom}:

$$\mu_{nom} \sim K\dot{\gamma}^{n-1} \sim K\left(\frac{\alpha}{L^2}\right)^{n-1}. \tag{5}$$

Eq. (5) gives rise to the following definitions of Rayleigh, Grashof and Prandtl numbers:

$$Ra = \frac{g\beta\Delta T L^{2n+1}}{\alpha^n (K/\rho)}; \quad Gr = \frac{g\beta\Delta T L^{4n-1}}{(K/\rho)^2 \alpha^{2n-2}} \quad \text{and} \quad Pr = \left(\frac{K}{\rho}\right)\alpha^{n-2} L^{2-2n}. \tag{6}$$

These definitions – which will be used for the remainder of this paper -are the same as those used by Ng and Hartnett [22] and Lamsaadi et al. [15,16]. However, a different definition of apparent dynamic viscosity was used earlier for analysing natural convection above a flat plate [23,24] and in a porous enclosure [25], which is given by:

$$\mu_K = \rho\left(\frac{K}{\rho}\right)^{\frac{1}{2-n}} L^{\frac{2(1-n)}{2-n}}. \tag{7}$$

Using Eq. (7) in Eqs. (3) and (4) yields the following definitions of Rayleigh and Prandtl numbers:

$$Ra_K = \frac{g\beta\Delta T L^3}{\alpha (K/\rho)^{1/(2-n)} H^{2(1-n)/(2-n)}}; \quad Pr_K = \frac{K L^{2-2n}}{\rho\alpha^{2-n}}. \tag{8}$$

Kim et al. [14] (hence the subscript "K") used the definitions given in Eq. (8) for their analysis of the current problem but the definitions given in Eq. (6) will be adopted in the current study following previous studies by Ng and Hartnett [22] and Lamsaadi et al. [15,16]. The Rayleigh (Prandtl) numbers Ra and Ra_K (Pr and Pr_K) are related in the following manner:

$$Ra = Ra_K Pr^{\frac{n-1}{2-n}} \quad \text{and} \quad Pr = Pr_K^{2-n}. \tag{9}$$

Both Ra and Ra_K (Pr and Pr_K) are valid definitions for nominal Rayleigh (Prandtl) numbers because the apparent viscosity μ_a is a local property which varies throughout the flowfield and cannot be adequately characterised by a single representative value. The relative merits of the definitions given by Eqs. (6) and (8) for the current configuration will be addressed later in Section 4.3.

Using dimensional analysis it is possible to show that for natural convection of power-law fluids in square enclosures: $Nu = f_1(Ra, Pr, n)$ where the Nusselt number Nu is given by:

$$Nu = \frac{hL}{k}, \tag{10}$$

where Nu represents the ratio of heat transfer rate by convection to that by conduction in the fluid in question and the heat transfer coefficient h is defined as:

$$h = \frac{k}{|T_{wall} - T_{ref}|}\left|\frac{\partial T}{\partial x}\right|_{wf}, \tag{11}$$

where subscript 'wf' refers to the condition of the fluid in contact with the wall, T_{wall} is the wall temperature and T_{ref} is the appropriate reference temperature, which can be taken to be T_C (T_H) for the hot (cold) wall respectively.

2.2. Numerical implementation

The commercial package FLUENT is used to solve the coupled conservation equations of mass, momentum and energy. This commercial package has been used successfully in a number of recent studies to simulate both inelastic power-law fluids [26] and Bingham fluids [20,21]. In this framework, a second-order central differencing is used for the diffusive terms and a second-order up-wind scheme for the convective terms. Coupling of the pressure and velocity is achieved using the well-known SIMPLE (Semi-Implicit Method for Pressure-Linked Equations) algorithm [27]. The convergence criteria in FLUENT were set to 10^{-9} for all the relative (scaled) residuals.

2.3. Governing equations

For the present study steady-state flow of an incompressible power-law fluid is considered. For incompressible fluids the conservation equations for mass, momentum and energy under steady-state take the following form:

Mass conservation equation

$$\frac{\partial u_i}{\partial x_i} = 0, \tag{12}$$

Momentum conservation equation

$$\rho u_j \frac{\partial u_i}{\partial x_j} = -\frac{\partial p}{\partial x_i} + \rho g \delta_{i2}\beta(T - T_C) + \frac{\partial \tau_{ij}}{\partial x_j}, \tag{13}$$

Energy conservation equation

$$\rho u_j c_p \frac{\partial T}{\partial x_j} = \frac{\partial}{\partial x_j}\left(k\frac{\partial T}{\partial x_j}\right), \tag{14}$$

where the cold wall temperature T_C is taken to be the reference temperature for evaluating the buoyancy term $\rho g \delta_{i2}\beta(T - T_C)$ in the momentum conservation equations following several previous studies [14,19–21]. The Kronecker's delta δ_{i2} in the source term $\rho g \delta_{i2}\beta(T - T_C)$ ensures that this term remains operational only for the momentum transport in the vertical direction (i.e. x_2-direction). The stress tensor is evaluated using Eq. (1).

2.4. Boundary conditions

The simulation domain is shown schematically in Fig. 1 where the two vertical walls of a square enclosure are kept at different temperatures ($T_H > T_C$), whereas the other boundaries are considered to be adiabatic in nature. Both velocity components (i.e. u_1 and u_2) are identically zero on each boundary because of the no-slip condition and impenetrability of rigid boundaries. The temperatures for hot and cold vertical walls are specified (i.e. $T(x_1 = 0) = T_C$ and $T(x_1 = L) = T_H$. The temperature boundary conditions for the horizontal insulated boundaries are given by: $\partial T/\partial x_2 = 0$ at $x_2 = 0$ and $x_2 = L$. Here 4 governing equations (1 continuity + 2 momentum + 1 energy) for 4 quantities (u, v, p, T) are solved and thus no further boundary conditions are needed for pressure.

2.5. Grid independency study

The grid independence of the results has been established based on a careful analysis of three different non-uniform meshes M1 (50 × 50), M2 (100 × 100) and M3 (200 × 200) and the relevant details, such as normalised minimum grid spacing $\Delta_{\min,cell}/L$ and grid expansion ratio r_e, are presented in Table 1. The numerical uncertainty is quantified in Table 2 using Richardson's extrapolation theory [28] for representative simulations of Newtonian (i.e. $n = 1$), shear thinning (i.e. $n = 0.6$) and shear thickening (i.e. $n = 1.8$) fluids at $Ra = 10^6$ and $Pr = 100$). The $n = 0.6$ and $n = 1.8$ data represent "extreme" scenarios for the power-law simulations shown here: the uncertainties quoted thus demonstrate the range for the data shown in the paper. For a general primitive variable ϕ the general Richardson extrapolation grid-converged value is given by: $\phi_{h=0} = \phi_1 + (\phi_2 - \phi_1)/(r^p - 1)$ where ϕ_1 is obtained based on the finest grid and ϕ_2 is the solution based on the next level of coarse grid, r is the ratio between the coarse to fine grid spacings and p is the theoretical order of accuracy. In this analysis the apparent order was taken to be 2. The numerical uncertainties for the mean Nusselt number ($\overline{Nu}$) and the maximum non-dimensional vertical velocity magnitude on the horizontal mid-plane of the enclosure ($V_{\max}$) are presented in Table 2. It can be seen from Table 2 that the numerical uncertainty levels remain smaller than 1% for all meshes for the simulations involving Newtonian (i.e. $n = 1$) and shear-thickening (i.e. $n = 1.8$) fluids. While the uncertainties for $\overline{Nu}$ in the $n = 0.6$ case remains comparable to that obtained for $n = 1.0$ and 1.8 cases, the uncertainty levels of $V_{\max}$ for the $n = 0.6$ case are considerably higher in comparison to the $n = 1.0$ and 1.8 cases. For the $n = 0.6$ case the uncertainty levels for $V_{\max}$ are 12%, 4% and 1% for meshes M1, M2 and M3 respectively. Based on the aforementioned uncertainty levels, the simulations were conducted using mesh M2 which provided a reasonable compromise between high accuracy and computational efficiency.

2.6. Benchmark comparison

In addition to the aforementioned grid-dependency study, the simulation results for Newtonian fluids (i.e. $n = 1.0$) have also been compared against the well-known benchmark data of de Vahl Davis [1] for Rayleigh numbers Ra ranging from 10^3 to 10^6 and Prandtl number equal to $Pr = 0.71$. The comparisons between the present simulation results for Newtonian fluids with the corresponding benchmark values were found to be excellent and entirely consistent with aforementioned grid-dependency analysis.

As an additional benchmark comparison, simulations for power-law fluids in the current configuration have been carried out for $Ra_K = 10^5{-}10^7$ and $Pr_K = 10^2{-}10^4$ and a comparison of $\overline{Nu}/\overline{Nu}_{n=1}$ values obtained from the present simulation results and the values reported in Kim et al. [14] is shown in Fig. 2. The agreement between the present results and the data reported in Kim et al. [14] is excellent across the entire Rayleigh and Prandtl number range for all values of n (note: Ref. [14] only report data for Newtonian and shear-thinning fluids, i.e. $n \leqslant 1$).

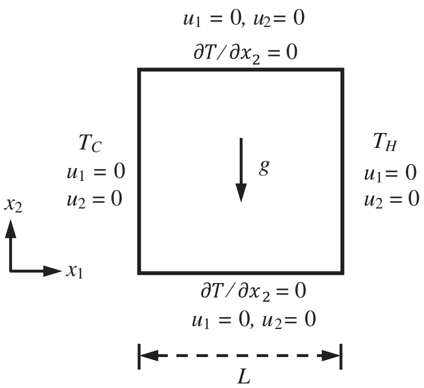

Fig. 1. Schematic diagram of the simulation domain.

Table 1
Non-dimensional minimum cell distance ($\Delta_{\min,cell}/L$) and grid expansion ratio (r_e) values for different meshes.

Grid	M1 (50 × 50)	M2 (100 × 100)	M3 (200 × 200)
$\Delta_{\min,cell}/L$	7.3921×10^{-3}	3.6960×10^{-3}	1.8480×10^{-3}
r_e	1.0747	1.0361	1.0177

Table 2
Numerical uncertainty for mean Nusselt number $\overline{Nu}$ and maximum non-dimensional vertical velocity component $V_{\max}$ at the horizontal mid-plane (i.e. $y/H = 0.5$) for $Ra = 10^6$ and $Pr = 100$ for representative shear-thinning ($n = 0.6$), Newtonian ($n = 1$) and shear-thickening ($n = 1.8$) cases.

	$\overline{Nu}$			$V_{\max}$		
	M1	M2	M3	M1	M2	M3
$n = 0.6$						
φ	34.0492	33.6849	33.6359	2237.26	2450.00	2527.77
φ_{ext}		33.6196			2553.69	
e_{ext} (%)	1.28	0.194	0.0486	12.4	4.06	1.02
$n = 1$						
φ	9.1476	9.1751	9.1989	234.4305	235.4176	235.9544
φ_{ext}		9.2068			236.1333	
e_{ext} (%)	0.643	0.345	0.0862	0.721	0.303	0.0758
$n = 1.8$						
φ	2.5266	2.5431	2.5480	26.8884	26.9980	27.0944
φ_{ext}		2.5496			27.1265	
e_{ext} (%)	0.903	0.256	0.0641	0.878	0.474	0.119

3. Scaling analysis

A scaling analysis is performed to elucidate the anticipated effects of Rayleigh number, Prandtl number and power-law index on the Nusselt number for power-law fluids. The wall heat flux q can be scaled as:

$$q \sim k\frac{\Delta T}{\delta_{th}} \sim h\Delta T, \tag{15}$$

which gives rise to the following relation:

$$Nu \sim \frac{h \cdot L}{k} \sim \frac{L}{\delta_{th}} \quad \text{or} \quad Nu \sim \frac{L}{\delta} f_2(Ra, Pr, n), \tag{16}$$

where the thermal boundary-layer thickness δ_{th} is related to the hydrodynamic boundary-layer thickness δ in the following way: $\delta/\delta_{th} \sim f_2(Ra, Pr, n)$ where $f_2(Ra, Pr, n)$ is a function of Rayleigh number, Prandtl number and power-law index, which is expected to increase with increasing Prandtl number. In order to estimate the hydrodynamic boundary-layer thickness δ, a balance of inertial and viscous forces in the vertical direction (i.e. x_2-direction) is considered:

$$\rho\frac{\vartheta^2}{L} \sim \frac{\tau}{\delta}, \tag{17}$$

where ϑ is a characteristic velocity scale. For power-law fluids the shear stress τ can be estimated as: $\tau \sim K(\vartheta/\delta)^n$, which upon substitution into Eq. (17) gives:

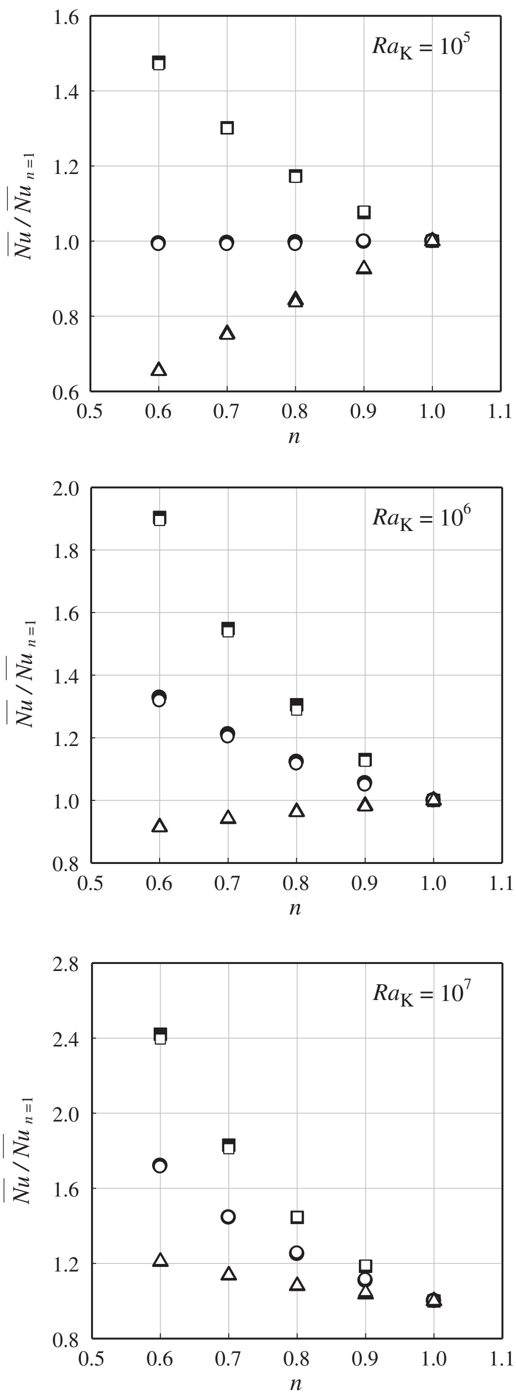

Fig. 2. Comparison of $\overline{Nu}/\overline{Nu}_{n=1}$ variation obtained from present simulation with the results obtained by Kim et al. [14] (white) for: (■) $Pr_K = 10^2$, (●) $Pr_K = 10^3$ and (▲) $Pr_K = 10^4$.

$$\rho \frac{\vartheta^2}{L} \sim K \frac{\vartheta^n}{\delta^{n+1}}. \tag{18}$$

Using Eq. (18) the hydrodynamic boundary-layer thickness can be estimated as:

$$\delta \sim \left(\frac{KL\vartheta^{n-2}}{\rho}\right)^{\frac{1}{n+1}}. \tag{19}$$

For natural convection the flow is induced by the buoyancy force and thus an equilibrium of inertial and buoyancy forces gives:

$$\frac{\vartheta^2}{L} \sim g\beta\Delta T. \tag{20}$$

This balance leads to an expression for the characteristic velocity scale:

$$\vartheta \sim \sqrt{g\beta\Delta TL}, \tag{21}$$

which can be used in Eq. (19) to yield:

$$\delta \sim \left[\frac{KL(g\beta\Delta TL)^{n/2-1}}{\rho}\right]^{\frac{1}{n+1}} \sim \frac{L}{(Ra^{2-n}Pr^{-n})^{\frac{1}{2(n+1)}}}, \tag{22}$$

where Ra and Pr are given by Eq. (6). This scaling gives rise to the following expression for the thermal boundary-layer thickness δ_{th}:

$$\delta_{th} \sim \min\left[L, \frac{1}{f_2(Ra, Pr, n)}\left(\frac{KL(g\beta\Delta TL)^{n/2-1}}{\rho}\right)^{\frac{1}{n+1}}\right] \sim \min\left[L, \frac{1}{f_2(Ra, Pr, n)} \frac{L}{(Ra^{2-n}Pr^{-n})^{\frac{1}{2(n+1)}}}\right]. \tag{23}$$

The above expression accounts for the fact the thermal boundary-layer thickness becomes of the order of the enclosure size L under very high values of n when conduction becomes the principal mode of heat transfer. Moreover, for a given set of values of Ra and Pr the thermal boundary-layer and hydrodynamic boundary-layer thicknesses (i.e. δ_{th} and δ) decrease with decreasing n. Eq. (23) suggests that δ_{th} decreases with increasing Ra for $n < 2$, which acts to increase the wall heat flux. Substitution of Eq. (23) into Eq. (15) yields:

$$\overline{Nu} \sim (Ra^{2-n}Pr^{-n})^{\frac{1}{2(n+1)}} f_2(Ra, Pr, n) \quad \text{when} \quad \overline{Nu} > 1. \tag{24}$$

The mean Nusselt number $\overline{Nu}$ attains a value equal to unity (i.e. $\overline{Nu} = 1.0$) when δ_{th} approaches to the enclosure size L. The scaling predictions provide useful insight into the anticipated behaviour of $\overline{Nu}$ in response to variations of Ra, Pr and n. Eq. (24) suggests that $\overline{Nu}$ is expected to decrease with increasing n for a given value of Ra when $n < 2$ whereas $\overline{Nu}$ increases with increasing Ra for a given value of n. It is also important to note that the mean Nusselt number $\overline{Nu}$ behaviour for Newtonian fluids can be obtained by setting $n = 1$ in Eq. (24). Doing so gives $\overline{Nu} \sim Ra^{0.25} f_2(Ra, Pr, 1)/Pr^{0.25}$ for Newtonian fluids whereas Berkovsky and Polevikov [29] proposed the correlation $\overline{Nu} = \int_0^L Nu \cdot dy/L = 0.18[RaPr/(0.2 + Pr)]^{0.29}$. Recently, Turan et al. [20] proposed a correlation for $\overline{Nu} = 0.162Ra^{0.293}[Pr/(1 + Pr)]^{0.091}$ which is also consistent with the scaling estimate shown in Eq. (24).

An apparent effective viscosity μ_{eff} can be estimated in the following way:

$$\mu_{eff} \sim K(\vartheta/\delta)^{n-1}. \tag{25}$$

Using Eqs. (21) and (22) in Eq. (25) yields:

$$\mu_{eff} \sim \rho\left(\frac{K}{\rho}\right)^{\frac{2}{n+1}} \frac{(g\beta\Delta TL)^{3(n-1)/2(n+1)}}{L^{(n-1)/(n+1)}}. \tag{26}$$

Eq. (26) can be used to estimate effective Grashof and Rayleigh numbers (i.e. Gr_{eff} and Ra_{eff}):

$$Gr_{eff} = \frac{\rho^2 g\beta\Delta TL^3}{\mu_{eff}^2} \sim Gr^{\frac{4-2n}{n+1}} Pr^{\frac{4(1-n)}{n+1}} \sim Ra^{\frac{4-2n}{n+1}} Pr^{\frac{-2n}{n+1}}, \tag{27}$$

$$Ra_{eff} = \frac{\rho^2 g\beta\Delta TL^3}{\mu_{eff}^2} \frac{\mu_{eff} c_p}{k} \sim Ra^{\frac{5-n}{2n+2}} Pr^{\frac{1-n}{2n+2}}. \tag{28}$$

The relations given by Eqs. (27) and (28) indicate that the effective values of Grashof and Rayleigh number become increasingly larger than their nominal values for decreasing values of n (especially

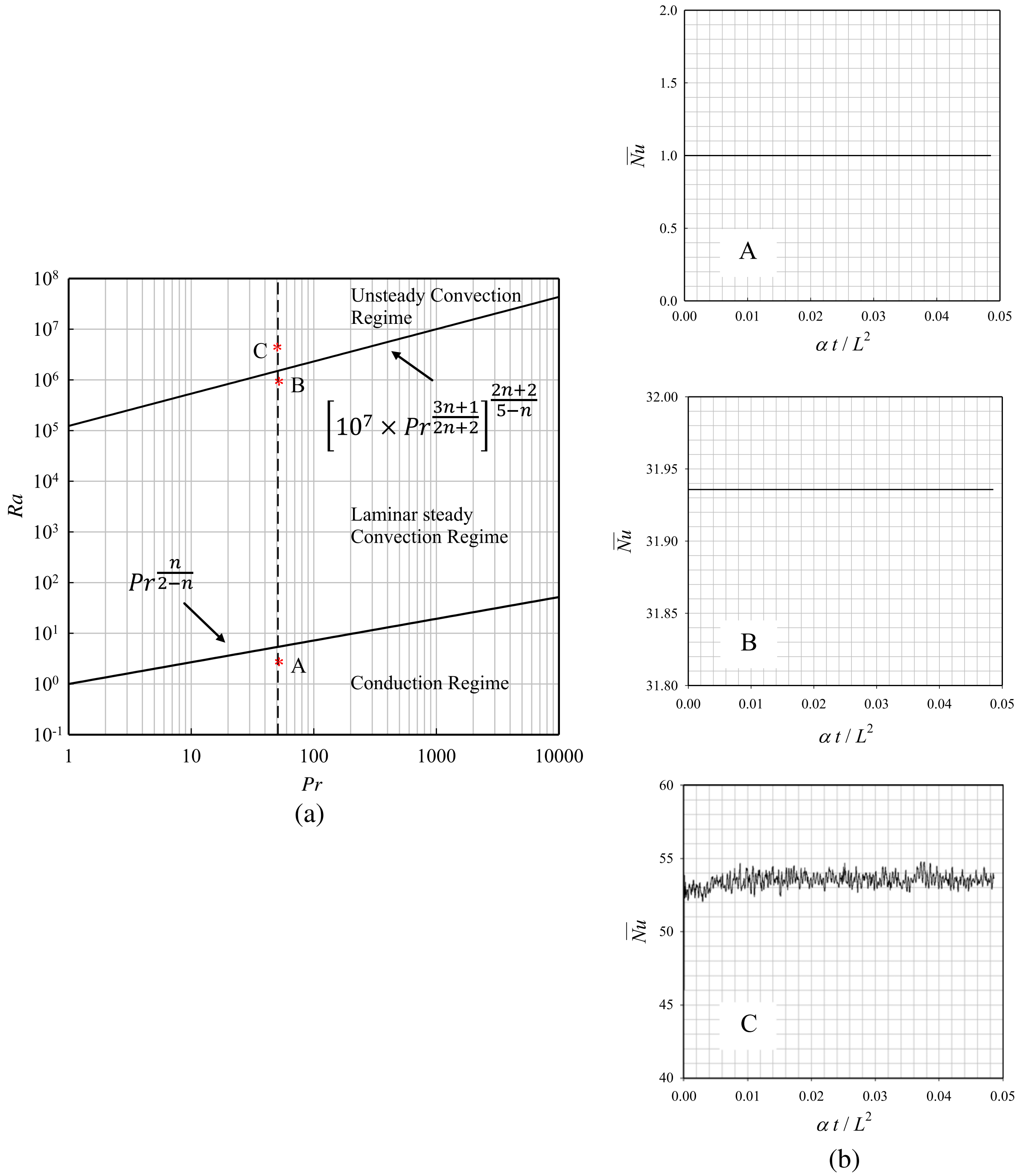

Fig. 3. (a) Different regimes of convection for $n = 0.6$, (b) Temporal evolution of $\overline{Nu}$ with dimensionless time $\alpha t/L^2$ at $Pr = 50$, $n = 0.6$ for: (A) conduction regime $Ra = 5$; (B) laminar steady convection regime $Ra = 1 \times 10^6$; and (C) unsteady convection regime $Ra = 5 \times 10^6$.

for $n < 1$). This suggests that for small values of n the magnitudes of Gr_{eff} and Ra_{eff} may attain such values that a steady two-dimensional laminar solution may not exist whereas a steady two-dimensional laminar solution can be obtained for the same set of nominal values of Ra and Pr for a higher value of n. Thus a critical value Ra_{crit} can be expected for the effective Rayleigh number Ra_{eff} such that a steady two-dimensional solutions cannot exist when $Ra_{eff} > Ra_{crit}$. A number of simulations have been carried out for different values of Ra, Pr and n and it has been found that converged two-dimensional steady solution cannot be obtained when $Ra_{eff} > 10^7 Pr$ and the critical effective Rayleigh number above which a steady solution can no longer be obtained is:

$$Ra_{crit} \sim Ra^{\frac{5-n}{2n+2}} Pr^{\frac{1-n}{2n+2}} = 10^7 Pr, \tag{29}$$

which essentially suggests that steady two-dimensional solutions do not exist for the following condition:

$$Ra > \left[10^7 Pr^{\frac{3n+1}{2n+2}}\right]^{\frac{2n+2}{5-n}}. \tag{30}$$

Moreover, a lower limit for Ra can be obtained using Eq. (24) above which convective transport plays a key role in heat transfer. For convective heat transfer to play an important role in the thermal transport, the mean Nusselt number $\overline{Nu}$ needs to exceed 1.0 (i.e. $\overline{Nu} > 1$) and thus the limiting condition for which convective heat transfer becomes important can be estimated as:

$$\overline{Nu} \sim (Ra^{2-n} Pr - n)^{\frac{1}{2(n+1)}} f_2(Ra, Pr, n) \sim 1.0. \tag{31}$$

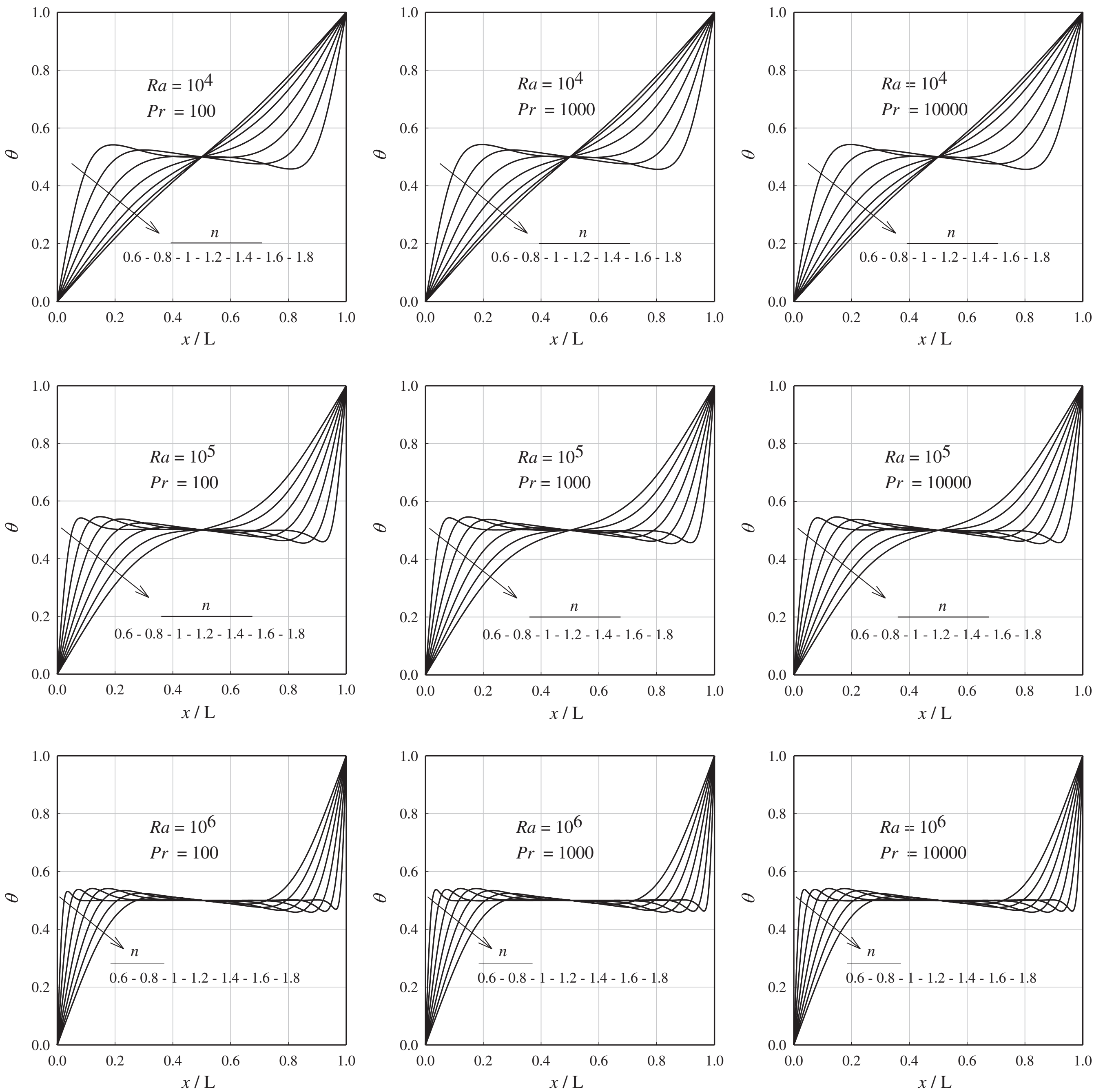

Fig. 4. Variations of non-dimensional temperature θ for $Pr = 100$ (left column), $Pr = 1000$ (middle column) and $Pr = 10{,}000$ (right column).

Considering $f_2(Ra, Pr, n) \sim 1.0$ one obtains the following limiting condition:

$$Ra \sim Pr^{\frac{n}{2-n}}. \qquad (32)$$

The conditions given by Eqs. (30) and (32) are shown in a regime diagram in Fig. 3a. When $Ra < Pr^{\frac{n}{2-n}}$ the heat transfer takes place principally due to thermal conduction and this regime is therefore called the 'conduction dominated regime' in Fig. 3a. The region given by $\left[10^7 Pr^{\frac{3n+1}{2n+2}}\right]^{\frac{2n+2}{5-n}} > Ra > Pr^{\frac{n}{2-n}}$ in Fig. 3a is termed as the 'steady laminar convection regime'. As steady two-dimensional laminar solutions do not exist for $Ra > \left[10^7 Pr^{\frac{3n+1}{2n+2}}\right]^{\frac{2n+2}{5-n}}$ the corresponding regime is referred to as the 'unsteady convection regime'. The validity of the above regime diagram can be substantiated from a series of unsteady calculations labelled as cases A, B and C on the regime diagram. For case A and B the mean Nusselt number $\overline{Nu}$ attains steady values (i.e. case A: $\overline{Nu} = 1.0$) as predicted by the regime diagram. The transient simulation for case C yielded a complex oscillation of $\overline{Nu}$ as observed from Fig. 3b. It is worth noting that non-convergence of steady state simulations does not necessarily indicate inexistence of a steady state (i.e. the non-convergence may be numerical in nature). Here the criteria given by Eqs. (29) and (30) for the critical condition above which a steady solution does not exist is confirmed by carrying out unsteady simulations for the parameters where a converged steady solution was not available (e.g. see case C in Fig. 3a and b).

It is important to note that the boundaries which distinguish one regime from another on the regime diagram shown in Fig. 3a

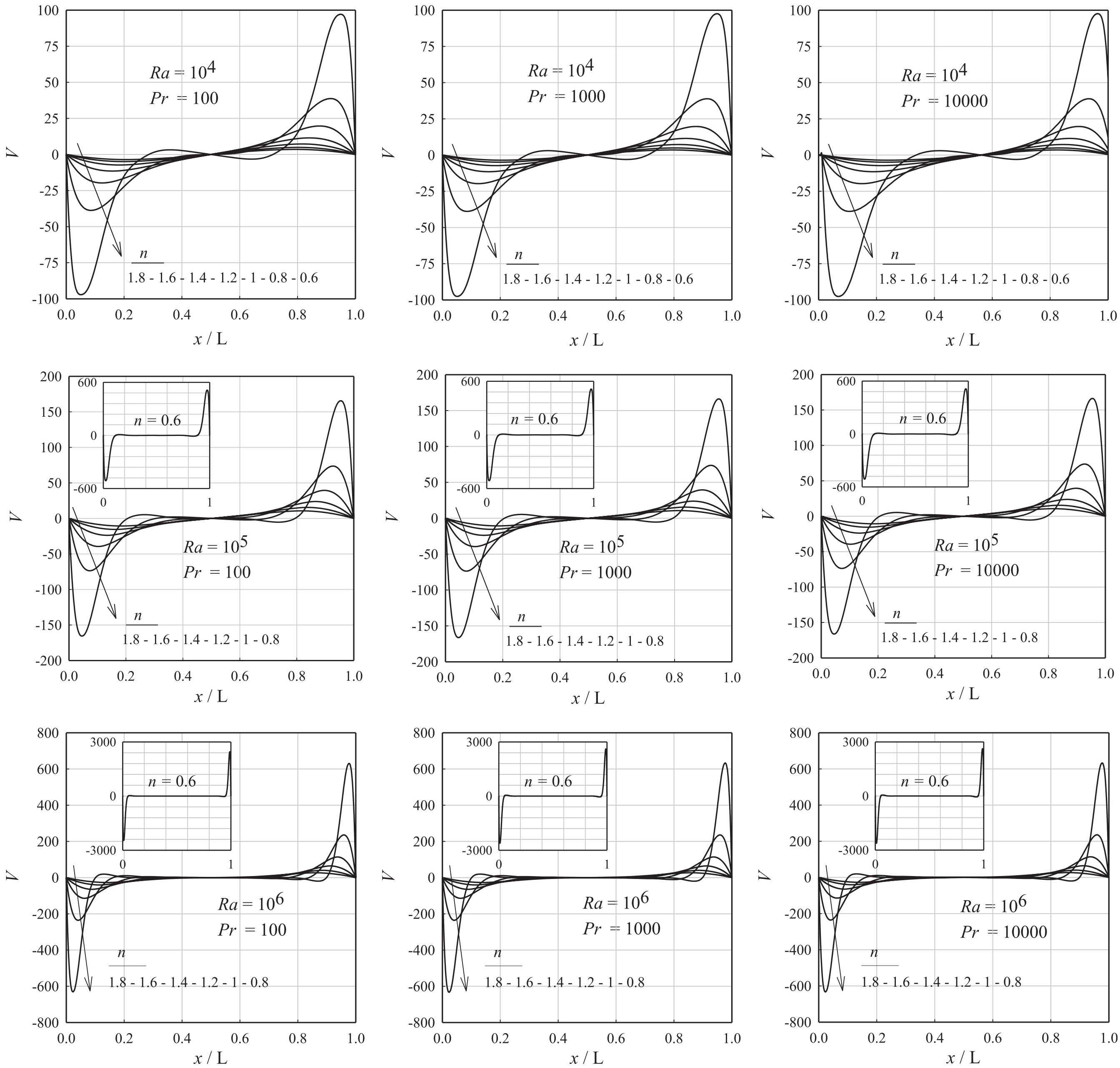

Fig. 5. Variations of non-dimensional vertical velocity component V for $Pr = 100$ (left column), $Pr = 1000$ (middle column) and $Pr = 10{,}000$ (right column).

are based on scaling arguments. As such these boundaries should not be treated rigidly but need to be considered only in an order of magnitude sense.

4. Results and discussion

4.1. Effects of power-law index n

It is useful to inspect the distributions of dimensionless temperature $\theta = (T - T_C)/(T_H - T_C)$ and the velocity components ($= u_i L/\alpha$) in order to understand the influences of n on the heat transfer rate during natural convection of power-law fluids in the square enclosure. The distributions of θ and $V = u_2 L/\alpha$ along the horizontal mid-plane (i.e. $x_2/L = 0.5$) for $Ra = 10^4$, 10^5 and 10^6 and $Pr = 10^2 - 10^5$ are shown in Figs. 4 and 5 respectively for different values of n ranging from 0.6 to 1.8. The distributions of $U = u_1 L/\alpha$ are not shown explicitly since, as a consequence of continuity, U and V remain of the same order of magnitude in a square enclosure (i.e. $U/L \sim V/L$). It is evident from Fig. 4 that the distributions of θ become increasing non-linear for decreasing values of n for a given set of values of Ra and Pr, which suggests that the effects of convection becomes increasingly strong for decreasing values of n when Ra and Pr are held constant. This statement is further supported by the data plotted in Fig. 5 which demonstrates that the magnitude of the velocity component increases significantly with decreasing power-law index when both Ra and Pr are kept unaltered. As Eq. (27) shows, for a given value of nominal Grashof number Gr, the effective Grashof number Gr_{eff} increases significantly with decreasing power-law index, which indicates that the strength of the buoyancy force becomes increasingly strong in comparison to viscous flow resistance for decreasing values of n and this effect is particularly prevalent for fluids with $n < 1$ because of shear thinning. On the other hand, the effects of

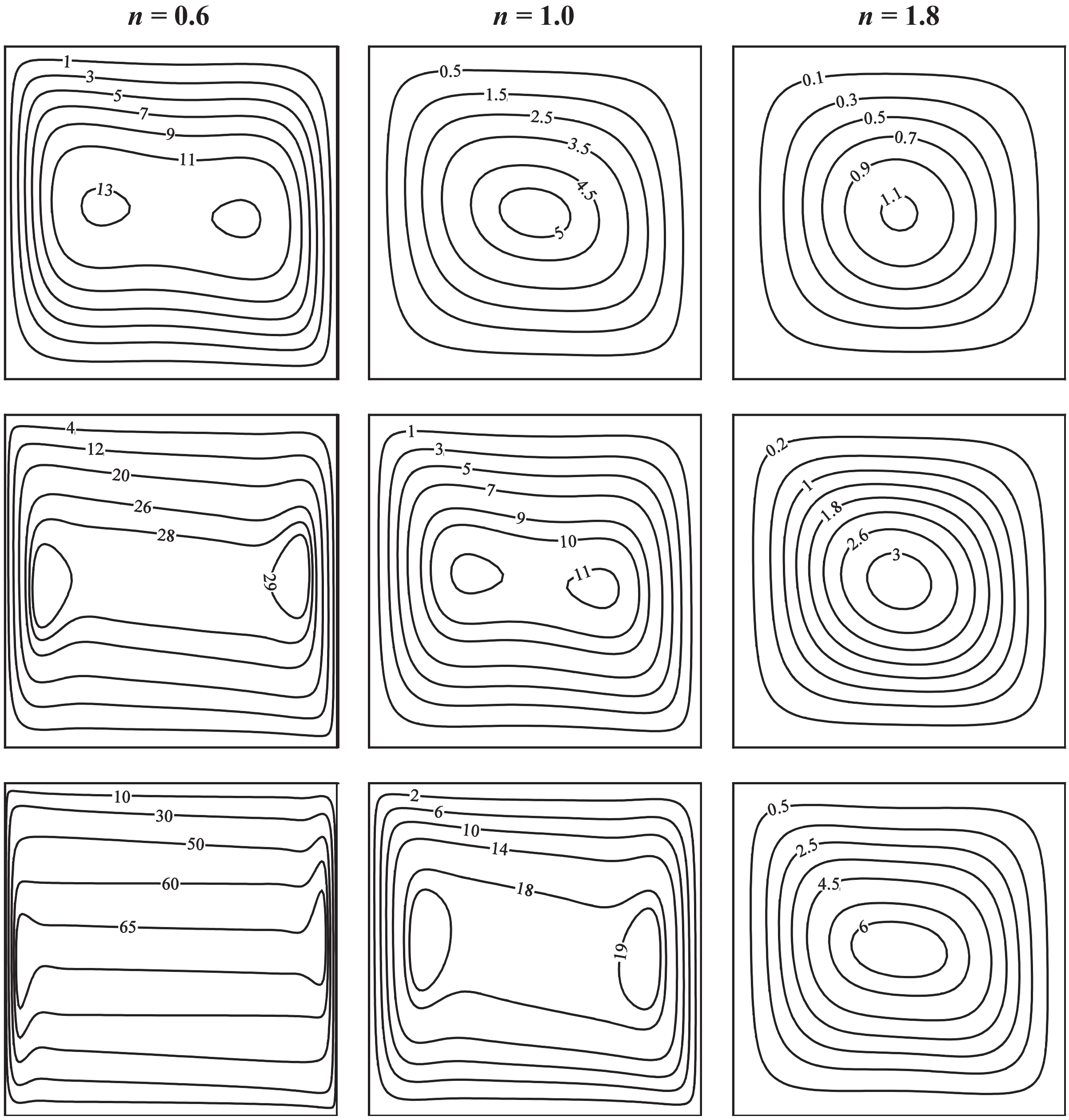

Fig. 6. Contours of non-dimensional stream functions ($\Psi = \psi/\alpha$) for n = 0.6, 1.0 and 1.8 for $Ra = 10^4$ (first row), $Ra = 10^5$ (second row) and $Ra = 10^6$ (third row) at Pr = 1000.

convection become increasingly weak in comparison to viscous forces with increasing n for shear-thickening fluids ($n > 1$). These effects of shear thickening can be seen in the small values of V and more linear distribution of θ for $n > 1$ fluids in Figs. 5 and 4 respectively. Especially for $Ra = 10^4$, conduction remains the principal mode of heat transport for $n = 1.8$ which can be seen from the almost linear distribution of θ and negligible magnitude of V (see Figs. 4 and 5). This finding is consistent with the scaling estimates given by Eq. (23) which indicates that δ_{th} may become of the order of L for large values of n and under this condition heat transfer becomes primarily conduction-driven, which is the case for $n = 1.8$ at $Ra = 10^4$. It can further be inferred from Eqs. (22) and (23) that both δ and δ_{th} become progressively thin with decreasing n when both Ra and Pr are kept constant: as can also be observed from the distributions of θ and V shown in Figs. 4 and 5. Moreover, the thinning of both hydrodynamic and thermal boundary layers with decreasing n can further be seen from the contours of dimensionless stream function $\Psi = \psi/\alpha$ and the isotherms shown in Figs. 6 and 7 respectively for $n = 0.6$, 1.0 and 1.8 at $Ra = 10^4$, 10^5 and 10^6, and $Pr = 10^3$. It can be observed from Fig. 6 that the magnitude of Ψ decreases (increases) with increasing (decreasing) n because of weakening (strengthening) of convective transport in comparison to viscous flow resistance. The isotherms also become progressively more curved with decreasing power-law index as a result of the strengthening of convective transport.

A decrease in the thermal boundary-layer thickness δ_{th} gives rise to an increase in the magnitude of heat flux at the vertical wall (see Eq. (15)), which acts to enhance the mean Nusselt number $\overline{Nu}$ as can be seen in Fig. 8 where the variations of mean Nusselt number $\overline{Nu}$ with Ra are shown for different values of n at $Pr = 10^2,\ 10^3$ and 10^4. The results shown in Fig. 8 are consistent with the scaling estimate given by Eq. (24) which suggests that $\overline{Nu}$ increases with decreasing n for a given set of values of Ra and Pr. This behaviour is also qualitatively consistent with the findings of Lamsaadi et al.

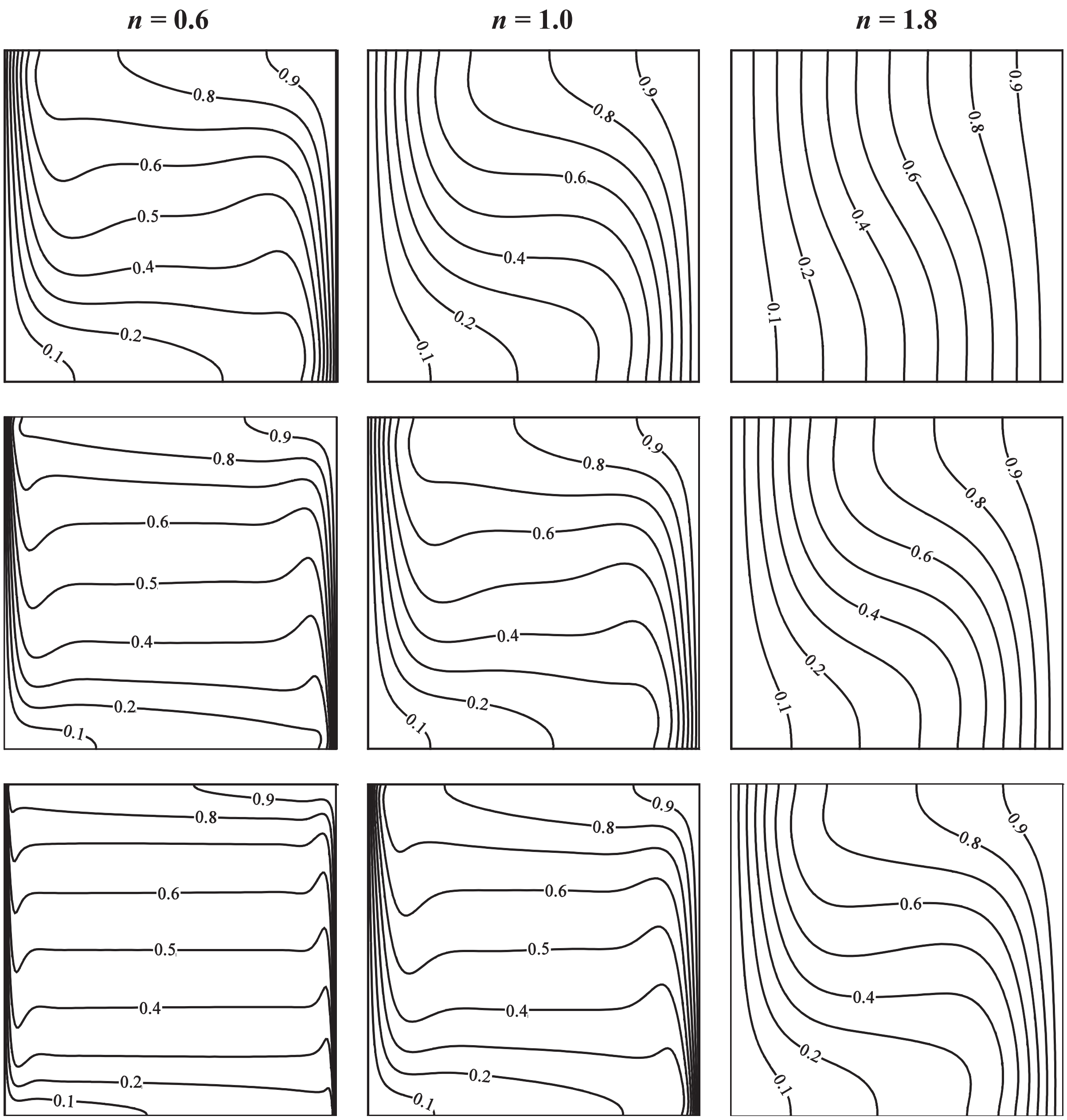

Fig. 7. Contours of non-dimensional temperature θ for n = 0.6, 1.0 and 1.8 for $Ra = 10^4$ (first row), $Ra = 10^5$ (second row) and $Ra = 10^6$ (third row) at Pr = 1000.

[15,16] for the same configuration with vertical walls subjected to constant heat flux instead of constant temperature.

4.2. Effects of nominal Rayleigh number Ra

For a given set of values of n and Pr an increase in Ra gives rise to strengthening of buoyancy forces in comparison to viscous forces which can be seen from Fig. 5 where the magnitude of V increases with increasing Ra. This enhancement of fluid velocity magnitude is consistent with the fact that the effective Grashof and Rayleigh numbers (i.e. Gr_{eff} and Ra_{eff}) increase with increasing Ra for a given set of values of n and Pr. As the convective transport strengthens with increasing Ra the distribution of θ becomes significantly more non-linear with increasing Ra (see the profiles in Fig. 4). For example, at $Ra = 10^4$ the thermal transport takes place principally due to conduction for $n = 1.8$ and this is reflected in the almost linear distribution of θ and negligible magnitude of V (see Figs. 4 and 5). However, the distribution of θ becomes non-linear and the magnitude of V rises with increasing Ra as evident from Figs. 4 and 5. Figs. 6 and 7 also show that the effects of convection strengthen with increasing Ra which is reflected in the augmentation in the magnitude of Ψ and progressively curved isotherms for higher values of Rayleigh number. It is clear from Figs. 4–7 that both δ and δ_{th} decrease with increasing Ra (for a given set of values of n and Pr) which is consistent with the scaling estimates given by Eqs. (22) and (23). The thinning of δ_{th} for larger values of Ra acts to enhance the magnitude of wall heat flux for the vertical walls (as Eqs. (15) and (16) show), which gives rise to an increase in $\overline{Nu}$. The increase in $\overline{Nu}$ with increasing Ra when n and Pr are kept unaltered for the range of values considered here is demonstrated in Fig. 8 which is also consistent with the scaling estimate given by Eq. (24). The Rayleigh number dependence of $\overline{Nu}$ for different values of n is found to be qualitatively consistent with the earlier results by Lamsaadi et al. [15,16] for the constant wall heat flux configuration.

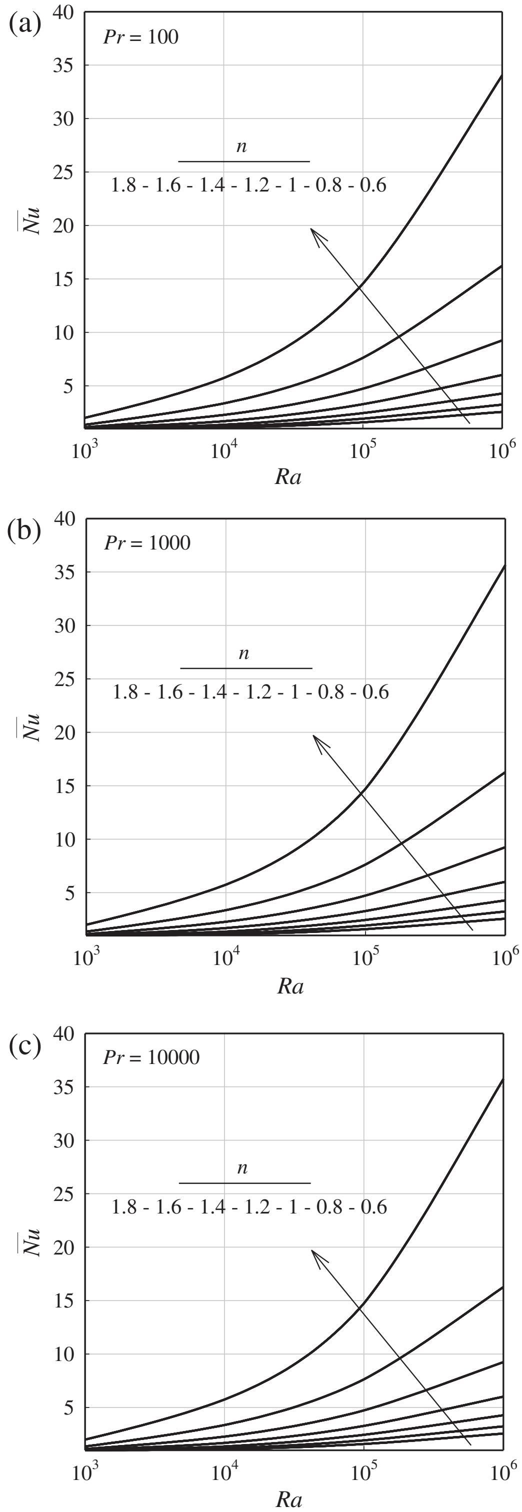

Fig. 8. The variation of the mean Nusselt number and Rayleigh number for different values of power law index n for: (a) $Pr = 100$, (b) $Pr = 1000$ and (c) $Pr = 10{,}000$.

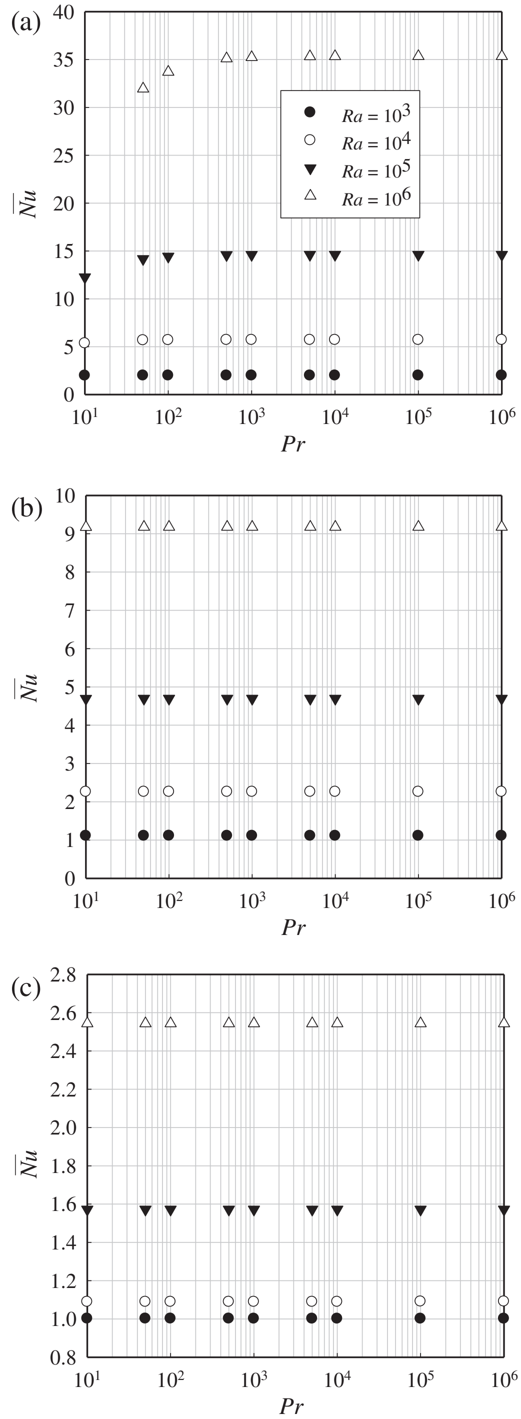

Fig. 9. The variation of the mean Nusselt number with Prandtl number for: (a) $n = 0.6$, (b) $n = 1.0$ and (c) $n = 1.8$.

4.3. Effects of nominal Prandtl number *Pr*

The effects of nominal Prandtl number Pr, in the range $Pr = 10–10^5$, have been explored in the present analysis for $Ra = 10^3–10^6$ and $n = 0.6–1.8$ as shown in Fig. 9. The value of $\overline{Nu}$ for $Pr = 10$ $Ra = 10^6$ and $n = 0.6$ is not shown in Fig. 9 because no steady-state converged solution could be obtained for these conditions. It is evident from Figs. 4 and 5 that the changes in Pr do not affect the distributions of θ and V and thus Pr does not have a major influence on the value of $\overline{Nu}$ in the range of Prandtl number considered here. This is consistent with earlier findings in the context of Newtonian fluids (i.e. $n = 1$) which demonstrated weak Pr dependence of $\overline{Nu}$ for $Pr \gg 1$ [4,5]. For $Pr \gg 1$ the hydrodynamic boundary-layer thickness remains much greater than the thermal boundary-layer thickness and as a result a change in Prandtl number principally modifies the relative balance between viscous and buoyancy forces so the heat transport in the thermal boundary-layer gets only marginally affected. This marginal modification of

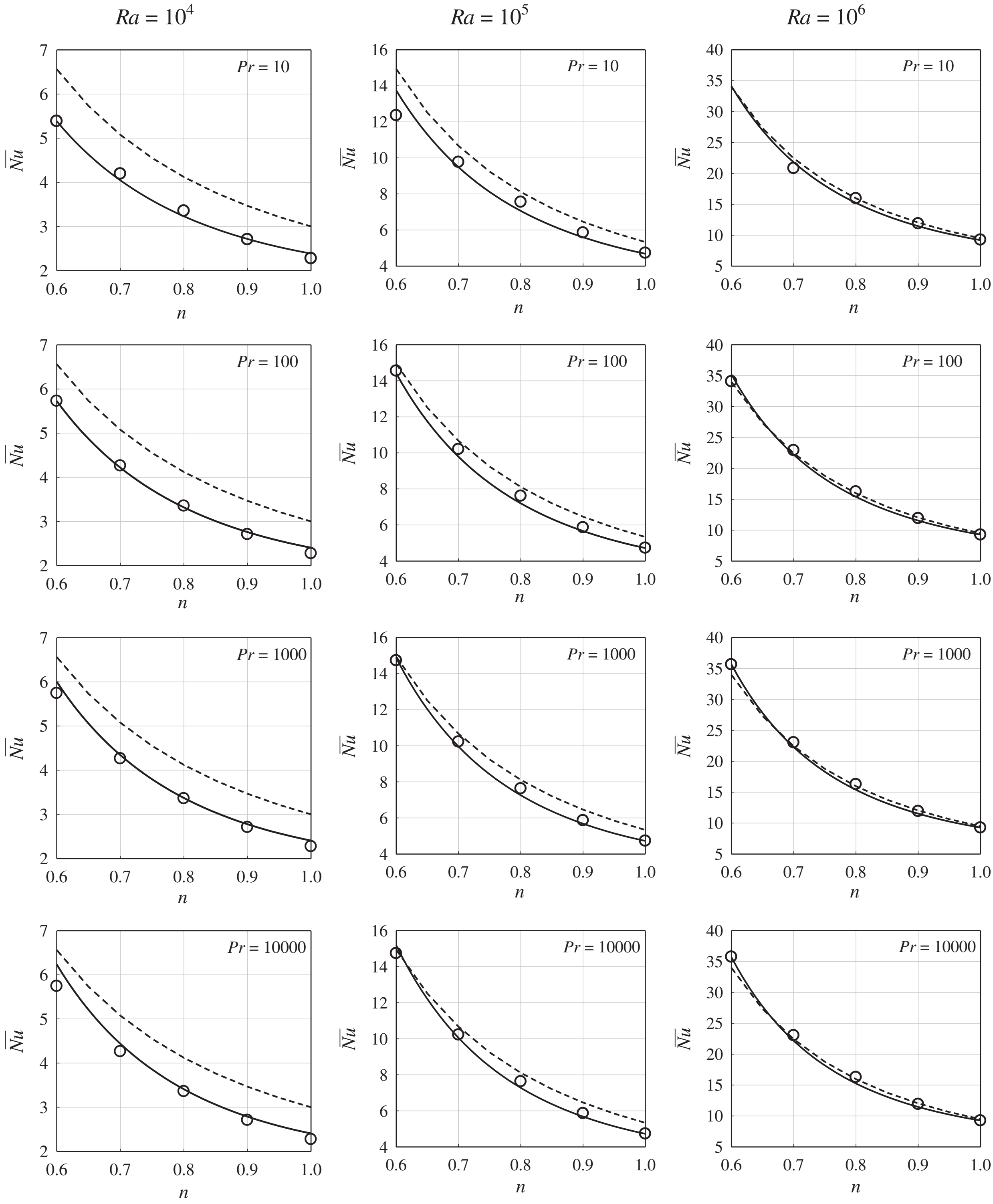

Fig. 10. Variations of $\overline{Nu}$ with power law index, $n \leqslant 1$ (○) for different values of Pr and Ra along with the predictions of Eq. (33) (—) and the correlation proposed by Kim et al. [14], Eq. (33v) (- - -).

thermal boundary-layer thickness is reflected in the weak Prandtl number dependence of $\overline{Nu}$ for large values of Pr in Fig. 9. Both the hydrodynamic and thermal boundary-layer thicknesses remain the thinnest for $Ra = 10^6$ and $n = 0.6$ amongst the cases studied here and thus a change in Pr alters the thermal boundary-layer thickness relatively significantly for these conditions. Consequently an increase in $\overline{Nu}$ is observed because an increase in Pr acts to decrease the thermal boundary-layer thickness.

The value of mean Nusselt number $\overline{Nu}$ is enhanced with increased shear thinning (i.e. decreasing n) for all values of nominal Rayleigh Ra and Prandtl Pr numbers considered in this study (see Figs. 8 and 9), which is consistent with the results of Lamsaadi et al. [15,16] for the constant heat flux configuration. In contrast, Kim et al. [14] reported non-monotonic variations with a growth in $\overline{Nu}$ with increasing n for $Pr_K = 10^4$ at $Ra_K = 10^5$ and 10^6 but with decreasing n for $Ra_K = 10^7$ (see

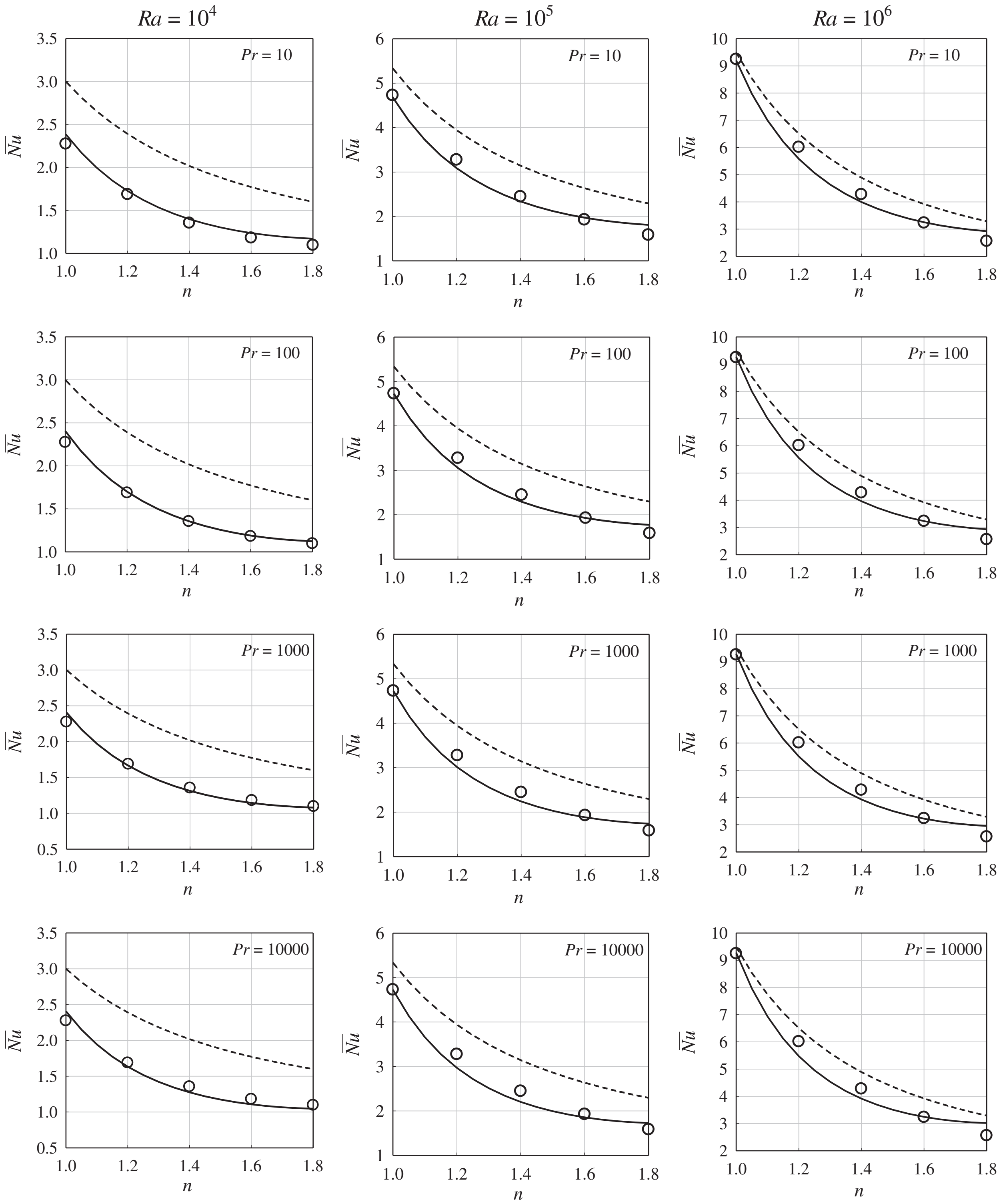

Fig. 11. Variations of $\overline{Nu}$ with power law index, $n > 1$ (○) for different values of Pr and Ra along with the predictions of Eq. (33) (—) and the correlation proposed by Kim et al. [14], Eq. (33v) (- - -).

Fig. 2 where these data are faithfully reproduced using the present numerical approach). As can be seen from Eq. (9), $Ra = Ra_K Pr_K^{n-1}$ and $Gr = Ra/Pr = Ra_K Pr_K^{2n-3}$ which indicates that both Ra and Gr decrease with decreasing values of n for a given set of values of Ra_K and Pr_K, and this tendency is particularly prevalent for the combination of small values of n and Ra_K and large value of Pr_K. This rapid reduction in Ra and Gr with decreasing n for a combination of small Ra_K and large Pr_K suggests weakening of buoyancy forces with respect to viscous forces, which ultimately leads to a reduction of $\overline{Nu}$ due to diminishing convection strength.

4.4. Correlation for mean Nusselt number $\overline{Nu}$

According to Eq. (24) the mean Nusselt number can be taken to scale with $\overline{Nu} \sim (Ra^{2-n} Pr^{-n})^{\frac{1}{2(n+1)}} f_2(Ra, Pr, n)$ and recently Turan et al.

[20] demonstrated that $\overline{Nu} = 0.162Ra^{0.293}[Pr/(1+Pr)]^{0.091}$ satisfactorily captures the Ra and Pr dependences of $\overline{Nu}$ for Newtonian fluids and thus the correlation for $\overline{Nu}$ for power-law fluids should be proposed in such a manner that $\lim_{n\to 1}\overline{Nu} = 0.162Ra^{0.293}[Pr/(1+Pr)]^{0.091}$. It has been shown earlier in Fig. 8 that $\overline{Nu}$ in power-law fluids with $n<1$ $(n>1)$ attains greater (smaller) values than the value of mean Nusselt number obtained for Newtonian fluids (i.e. $n=1$) for the same nominal values of Ra and Pr. Based on the aforementioned observations and limiting conditions a correlation for $\overline{Nu}$ is proposed here in the following manner:

$$\overline{Nu} = 0.162Ra^{0.043}\frac{Pr^{0.341}}{(1+Pr)^{0.091}}\left(\frac{Ra^{2-n}}{Pr^{n}}\right)^{\frac{1}{2(n+1)}} e^{b(n-1)}, \tag{33i}$$

where b is a correlation parameter which can be expressed based on simulation results as:

$$b = c_1 Ra^{c_2} Pr^{c_3}, \tag{33ii}$$

where $c_1,\ c_2$ and c_3 are given by:

$$c_1 = 1.343;\quad c_2 = 0.065 \quad \text{and} \quad c_3 = 0.036 \quad \text{for } n \leqslant 1, \tag{33iii}$$

$$c_1 = 0.858;\quad c_2 = 0.071 \quad \text{and} \quad c_3 = 0.034 \quad \text{for } n > 1. \tag{33iv}$$

According to Eqs. (33)i–iv the expression of $\overline{Nu}$ becomes exactly equal to an existing correlation for Newtonian fluids (i.e. $\overline{Nu} = 0.162Ra^{0.293}[Pr/(1+Pr)]^{0.091}$ in Ref. [20]) when n is taken to be unity (i.e. $n=1$). Kim et al. [14] also proposed a correlation for $\overline{Nu}$ in the current configuration based on computational simulations of power-law fluids for $10^6 \leqslant Ra_K \leqslant 10^7$, $10^2 \leqslant Pr_K \leqslant 10^4$ and $0.6 \leqslant n \leqslant 1.0$:

$$\overline{Nu} = 0.3n^{0.4}\left(Ra_K Pr_K^{n-1}\right)^{\frac{1}{3n+1}} = 0.3n^{0.4}(Ra)^{\frac{1}{3n+1}}. \tag{33v}$$

The quality of the correlations given by Eqs. (33) and (33v) for fluids with $n \leqslant 1$ for $Ra = 10^4$–10^6 and $Pr = 10^2$–10^4 are shown in Fig. 10. The performance of these correlations for the aforementioned range of Rayleigh and Prandtl numbers are shown in Fig. 11 for $n>1$ fluids. It can be seen from Figs. 10 and 11 that Eq. (33) satisfactorily predicts the qualitative and quantitative behaviour of $\overline{Nu}$ across all power-law indices considered here. Figs. 10 and 11 demonstrate that although the correlation proposed by Kim et al. [14] (Eq. (33v)) satisfactorily captures the qualitative variation of $\overline{Nu}$, this correlation overpredicts the value of $\overline{Nu}$ for all the cases considered here. The extent of this overprediction is particularly prevalent for small values of Ra and the accuracy of its prediction improves with increasing Ra. For large values of Ra (e.g. $Ra = 10^6$) the predictions of Eqs. (33) and (33v) remain comparable for shear-thinning fluids. It is worth noting that the correlation given by Eq. (33v) was originally proposed for $10^6 \leqslant Ra_K \leqslant 10^7$, $10^2 \leqslant Pr_K \leqslant 10^4$ and $0.6 \leqslant n \leqslant 1.0$ and thus the overprediction of $\overline{Nu}$ for a broader range of Ra, Pr (i.e. Ra_K, Pr_K) and n is perhaps not unexpected. Based on the observations from Figs. 10 and 11 the correlation given by Eq. (33) is recommended here for $10^4 \leqslant Ra \leqslant 10^6$, $10 \leqslant Pr \leqslant 10^5$ and $0.6 \leqslant n \leqslant 1.8$.

5. Conclusions

In this study, the heat transfer characteristics of two-dimensional steady laminar natural convection of power-law fluids in a square enclosure with differentially heated side walls subjected to constant wall temperatures have been numerically studied. The effects of Rayleigh number Ra, Prandtl number Pr and power-law index n on heat and momentum transport have been systematically investigated. The results show that the mean Nusselt number $\overline{Nu}$ rises with increasing values of the Rayleigh number for both Newtonian and power-law fluids. The Nusselt number was found to decrease with increasing power-law index n, and, for large values of n, the value of mean Nusselt number settled to unity (i.e. $\overline{Nu} = 1$) as the heat transfer took place principally by conduction.

The simulation results show that the mean Nusselt number $\overline{Nu}$ is marginally affected by the increase in Pr for Newtonian and power-law fluids for a given set of values of the Rayleigh number Ra and power law index n. Finally, guided by a scaling analysis, the simulation results are used to propose a new correlation for $\overline{Nu}$ for power-law fluids with n ranging from 0.6 to 1.8. This correlation is shown to satisfactorily capture the variation of $\overline{Nu}$ with Ra, Pr and n for all the cases considered in this study. Moreover, this correlation reduces to an existing correlation for $\overline{Nu}$ for Newtonian fluids when $n=1$.

It is important to note that in the present study the temperature dependences of thermo-physical properties such as consistency and thermal conductivity have been neglected as a first step to aid the fundamental understanding of natural convection in power-law fluids in square enclosures with differentially heated side walls subjected to constant wall temperatures. Although the inclusion of temperature-dependent thermo-physical properties are not expected to change the qualitative behaviour observed in the present study, the inclusion of temperature dependence of consistency K, power-law index n and thermal conductivity k is probably necessary for quantitative predictions. Thus future investigation on the same configuration with temperature-dependent thermo-physical properties of power law fluids will be necessary for deeper understanding and more accurate quantitative predictions.

References

[1] G. de Vahl Davis, Natural convection of air in a square cavity: a bench mark numerical solution, Int. J. Numer. Meth. Fluids 3 (1983) 249–264.

[2] A.F. Emery, J.W. Lee, The effects of property variations on natural convection in a square cavity, J. Heat Transfer 121 (1999) 57–62.

[3] O. Aydın, A. Ünal, T. Ayhan, Natural convection in rectangular enclosures heated from one side and cooled from above, Int. J. Heat Mass Transfer 42 (1999) 2345–2355.

[4] S. Ostrach, Natural convection in enclosures, J. Heat Transfer 110 (1988) 1175–1190.

[5] A. Bejan, Convection Heat Transfer, John Wiley Sons Inc., New York, 1984.

[6] H. Ozoe, S.W. Churchill, Hydrodynamic stability and natural convection in Ostwald–De Waele and Ellis fluids: the development of a numerical solution, AIChE J. 18 (1972) 1196–1207.

[7] M. Lamsaadi, M. Naïmi, M. Hasnaoui, Natural convection of non-Newtonian power law fluids in a shallow horizontal rectangular cavity uniformly heated from below, Heat Mass Transfer 41 (2005) 239–249.

[8] M. Ohta, M. Akiyoshi, E. Obata, A numerical study on natural convective heat transfer of pseudo-plastic fluids in a square cavity, Numer. Heat Transfer A 41 (2002) 357–372.

[9] H. Inaba, C. Daib, A. Horibe, Natural convection heat transfer of microemulsion phase-change material slurry in rectangular cavities heated from below and cooled from above, Int. J. Heat Mass Transfer 46 (2003) 4427–4438.

[10] J. Zhang, D. Vola, I.A. Frigaard, Yield stress effects on Rayleigh–Bénard convection, J. Fluid Mech. 566 (2006) 389–419.

[11] N.J. Balmforth, A.C. Rust, Weakly nonlinear viscoplastic convection, J. Non-Newt. Fluid Mech. 158 (2009) 36–45.

[12] A. Vikhansky, Thermal convection of a viscoplastic liquid with high Rayleigh and Bingham numbers, Phys. Fluids 21 (2009) 101303.

[13] H.M. Park, D.H. Ryu, Rayleigh–Bénard convection of viscoelastic fluids in finite domains, J. Non-Newt. Fluid Mech. 98 (2001) 169–184.

[14] G.B. Kim, J.M. Hyun, H.S. Kwak, Transient buoyant convection of a power law non-Newtonian fluid in an enclosure, Int. J. Heat Mass Transfer 46 (2003) 3605–3617.

[15] M. Lamsaadi, M. Naïmi, M. Hasnaoui, M. Mamou, Natural convection in a vertical rectangular cavity filled with a non-Newtonian power law fluid and subjected to a horizontal temperature gradient, Numer. Heat Transfer Part A 49 (2006) 969–990.

[16] M. Lamsaadi, M. Naïmi, M. Hasnaoui, Natural convection heat transfer in shallow horizontal rectangular enclosures uniformly heated from the side and filled with non-Newtonian power law fluids, Energy Convers. Manage. 47 (2006) 2535–2551.

[17] W.L. Barth, G.F. Carey, On a natural-convection benchmark problem in non-Newtonian fluids, Numer. Heat Transfer Part B 50 (2006) 193–216.

[18] W.H. Leung, K.G.T. Hollands, A.P. Brunger, On a physically-realizable Benchmark problem in internal natural convection, Int. J. Heat Mass Transfer 41 (1998) 3817–3828.
[19] D. Vola, L. Boscardin, J.C. Latché, Laminar unsteady flows of Bingham fluids: a numerical strategy and some benchmark results, J. Comput. Phys. 187 (2003) 441–456.
[20] O. Turan, N. Chakraborty, R.J. Poole, Laminar natural convection of Bingham fluids in a square enclosure with differentially heated side walls, J. Non-Newt. Fluid Mech. 165 (2010) 903–913.
[21] O. Turan, R.J. Poole, N. Chakraborty, Aspect ratio effects in laminar natural convection of Bingham fluids in rectangular enclosures with differentially heated side walls, J. Non-Newt. Fluid Mech. 166 (2011) 208–230.
[22] M.L. Ng, J.P. Hartnett, Natural convection in power law fluids, Int. Commun. Heat Mass Transfer 13 (1986) 115–120.
[23] J. Dale, A. Emery, The free convection of heat from a vertical plate to several non-Newtonian pseudoplastic fluids, ASME J. Heat Transfer 94 (1972) 64–72.
[24] A. Acrivos, A theoretical analysis of laminar natural convection heat transfer to non-Newtonian fluids, AIChE J. 6 (1960) 584–590.
[25] G. Getachew, W. Mincowycz, D. Poulikakos, Natural convection in a porous cavity saturated with a non-Newtonian fluid, J. Thermophys. Heat Transfer 10 (1996) 640–651.
[26] R.J. Poole, B.S. Ridley, Development length requirements for fully-developed laminar pipe flow of inelastic non-Newtonian liquids, ASME J. Fluids Eng. 129 (2007) 1281–1287.
[27] S.V. Patankar, Numerical Heat Transfer and Fluid Flow, Hemisphere, Washington, DC, 1980.
[28] P.J. Roache, Quantification of uncertainty in computational fluid dynamics, Annu. Rev. Fluid Mech. 29 (1997) 123–160.
[29] B.M. Berkovsky, V.K. Polevikov, Numerical study of problems on high-intensive free convection, in: D.B. Spalding, H. Afgan (Eds.), Heat Transfer and Turbulent Buoyant Convection, Hemisphere, Washington, DC, 1977, pp. 443–455.